frontiers in Materials

ORIGINAL RESEARCH
published: 05 August 2021
doi: 10.3389/fmats.2021.736011

Intrinsic Complex Vacancy-Induced d^0 Magnetism in $Ca_2Nb_2O_7$ PLD Film

Linjie Wu[1], *Yongjia Zhang*[1], *Zhongquan Nie*[2] *and Ensi Cao*[1]*

[1]College of Physics and Optoelectronics, Taiyuan University of Technology, Taiyuan, China, [2]Key Lab of Advanced Transducers and Intelligent Control System, Ministry of Education, Taiyuan University of Technology, Taiyuan, China

Introducing magnetism into the ferroelectric $Ca_2Nb_2O_7$ with high Curie temperature can make it a potential multiferroic material at room temperature. Stoichiometric $Ca_2Nb_2O_7$, nonstoichiometric $Ca_{1.9}Nb_2O_{7-\delta}$ and $Ca_2Nb_{1.9}O_{7-\delta}$ single phase films were deposited on STO (110) substrate by pulsed laser deposition under appropriate conditions. The films were characterized by XRD, FE-SEM, Element mapping and XPS. Both stoichiometric $Ca_2Nb_2O_7$ and $Ca_{1.9}Nb_2O_{7-\delta}$ films were diamagnetic in the magnetic measurement and *ab initio* calculations, while the $Ca_2Nb_{1.9}O_{7-\delta}$ film with the complex vacancy of V_{Nb+O} exhibited ferromagnetic behavior at room temperature, with the saturated magnetization of 3.6 emu/cm^3. Calculations on the $Ca_2Nb_2O_7$ (010) surface indicate that the V_{Nb+O} can induce spin polarization on the residual O atoms around the Nb vacancies, and the system was most stable when the Nb and O vacancies were the 4th nearest-neighbored, with FM coupling energetically more stable than the AFM coupling. Our work verified experimentally and theoretically the feasibility of introducing ferromagnetism into $Ca_2Nb_2O_7$ film by the intrinsic complex vacancy of V_{Nb+O}.

Keywords: PLD, ab initio calculation, complex vacancy, Ca2Nb2O7, d0 magnetism

OPEN ACCESS

Edited by:
Han Lin,
Swinburne University of Technology, Australia

Reviewed by:
Tongshuai Xu,
Anyang Normal University, China
Feng Jiang,
Dalian University of Technology, China

****Correspondence:***
Ensi Cao
ECao@163.com

Specialty section:
This article was submitted to Quantum Materials, a section of the journal Frontiers in Materials

Received: *04 July 2021*
Accepted: *22 July 2021*
Published: *05 August 2021*

Citation:
Wu L, Zhang Y, Nie Z and Cao E (2021) Intrinsic Complex Vacancy-Induced d^0 Magnetism in $Ca_2Nb_2O_7$ PLD Film. Front. Mater. 8:736011. doi: 10.3389/fmats.2021.736011

INTRODUCTION

Multiferroic materials with the co-existance of ferroelectricity (FE) and ferromagnetism (FM) have received considerable attention in recent years due to the unique physical mechanism of magnetoelectric coupling and potential applications in the fields of information storage, processing and sensing (Fiebig, 2005; Chun et al., 2012). However, the natural conflict between FM and FE leads to the rarity of multiferroic material at room temperature (RT) (Hill, 2000). $Ca_2Nb_2O_7$ is a member of the $A_nNb_nO_{3n+2}$ family with n = 4, which has layered perovskite structure and high ferroelectric Curie temperature (above 1850°C) (Lichtenberg et al., 2001). The introduction of FM into ferroelectric $Ca_2Nb_2O_7$ could make it a potential multiferroic material at RT.

In order to achieve FM in ferroelectric materials, doping magnetic elements was the most frequently adopted method. So far, RTFM has been experimentally observed in the Fe-doped $BaTiO_3$ films (Ramana et al., 2013; Chand Verma et al., 2014), Fe-doped $LiTaO_3$ ceramics (Song et al., 2014) and Fe-doped $K_{0.45}Na_{0.49}Li_{0.06}NbO_3$ ceramics (Liu et al., 2015), the origin of which can be theoretically well explained by the F-center model for diluted magnetic semiconductors. Besides, nonmagnetic element doping induced d^0 magnetism has been observed in $BaTiO_3$ film/ceramics, Nb-doped $BaTiO_3$ film and $LiNbO_3$ nanocrystallites, the origin of which was ascribed to the oxygen vacancy (Mangalam et al., 2009; Yang et al., 2010; Díaz-Moreno et al., 2014). However, the observed FM in Eu-doped $CdNb_2O_6$ powders was elucidated with the intrinsic exchange interactions between the magnetic moments associated with the unpaired 4*f* electrons in Eu^{3+} ions (Topkaya et al., 2017). The RTFM in $K_{0.5}Na_{0.5}NbO_3$ PLD film was related to the cationic K and Na vacancies (Cao et al.,

2011a), while the RTFM observed in $BaNb_2O_6$ film was contributed mainly by the oxygen vacancy, with certain contribution by the Nb vacancy (Cao et al., 2012). In the aspect of theoretical study, both Ti and O vacancies were found to be able to induce FM in $BaTiO_3$ bulk material and (001) surface (Cao et al., 2009; Cao et al., 2011b) and in $PbTiO_3$ (Shimada et al., 2012). However, O vacancy was found to be able to induce FM in $LiNbO_3$ but cannot induce FM in $LiTaO_3$ and Sr_2AlNbO_6 (Cao et al., 2013; Li et al., 2014).

Therefore, the origin of FM in undoped ferroelectric material is still controversial in both experimental and theoretical results. Meanwhile, most of the analyses on the vacancy-induced d^0 magnetism in ferroelectric oxide films just considered various cation vacancies or oxygen vacancy alone, the synergistic effect of cation and oxygen vacancies, i.e., the effect of complex vacancy, was seldom studied. Herein, the advantage of the identical composition between the film and ceramic target in pulsed laser deposition (PLD) was utilized to prepare stoichiometric $Ca_2Nb_2O_7$ single phase film and those with the complex vacancy of V_{Ca+O} or V_{Nb+O} by varying the composition of $Ca_2Nb_2O_7$ ceramic targets. The probability of achieving d^0 magnetism in the nonstoichiometric $Ca_2Nb_2O_7$ single phase film by complex vacancy was comprehensively examined by magnetic measurement and ab initio calculations.

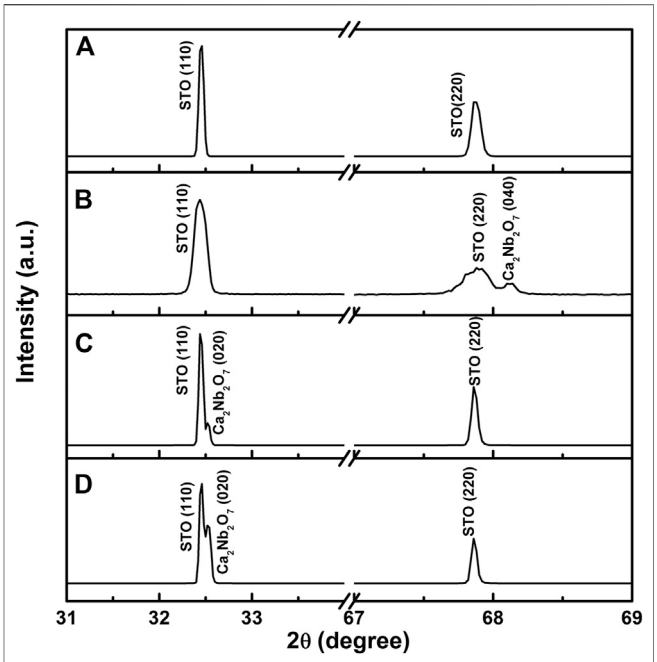

FIGURE 1 | XRD patterns of the STO substrate **(A)**, the as-deposited films using stoichiometric $Ca_2Nb_2O_7$ target **(B)**, nonstoichiometric $Ca_2Nb_2O_7$ target with 5% Ca deficiency **(C)** and Nb deficiency **(D)**.

MATERIALS AND METHODS

$CaCO_3$ and Nb_2O_5 were used as raw material and weighted according to the atomic ratio of Ca/Nb as 0.95/1, 1/1, and 1/0.95, respectively. Stoichiometric and nonstoichiometric $Ca_2Nb_2O_7$ ceramic targets with intrinsic cation vacancies were then obtained by the conventional solid state reaction. Ablation of the targets were achieved using a KrF excimer laser source (λ = 248 nm, pulse duration = 20 ns, energy of pulse = 200 mJ, frequency of pulse = 3 Hz). $SrTiO_3$ (110) substrate in the size of 5 mm × 5 mm was chosen due to its smaller lattice mismatch with the $Ca_2Nb_2O_7$ lattice. The deposition duration was 0.5 h, the distance between the target and substrate was 60 mm, the substrate temperature (T_S) was 650°C, and the oxygen pressure (P_O) was 1 mTorr for all depositions.

The crystal structure was examined by High Resolution X-ray Diffractometer (D8 discover, Bruker AXS GmbH, German) using Cu Kα radiation. The SEM and element mapping on the surface were performed by Scanning Electron Microscope (SU8010, Hitachi, Japan). X-ray photoelectron spectra were obtained by X-ray Photoelectron Spectrometer with monochromated Al Kα radiation (Escalab 250, Thermo Electron Corporation, United States). Magnetic properties were measured by Magnetic Property Measurement System (MPMS-5XL, Quantum design, United States) with magnetic field parallel to the surface of film. The film thickness was checked by Stylus Surface Profiler (Dektak 150, Veeco Metrology, France).

RESULTS AND DISCUSSION

Structural and Surface Characterizations

Figure 1 shows the XRD patterns of the STO substrate and the as-deposited films. Aside from the (110) and (220) diffraction peaks from the substrate (see **Figure 1A**), the only appearance of (040) diffraction peaks from orthorhombic $Ca_2Nb_2O_7$ (PDF#70-2006) in **Figure 1B** means that single phase of stoichiometric $Ca_2Nb_2O_7$ was obtained under the current deposition conditions without impurity phase. The $Ca_2Nb_2O_7$ (020) diffraction peaks in **Figures 1C,D** indicated that the single phase of $Ca_2Nb_2O_7$ was maintained using the targets with 5% Ca or Nb deficiency. To maintain the charge neutrality, the Ca or Nb vacancy would lead to the concomitant appearance of oxygen vacancy in the $Ca_2Nb_2O_7$ lattice, therefore, the nonstoichiometric $Ca_2Nb_2O_7$ films were denoted as $Ca_{1.9}Nb_2O_{7-\delta}$ and $Ca_2Nb_{1.9}O_{7-\delta}$, respectively. The film thickness of the three samples was close and approximated to be 100 nm. The SEM images for the $Ca_2Nb_2O_7$, $Ca_{1.9}Nb_2O_{7-\delta}$ and $Ca_2Nb_{1.9}O_{7-\delta}$ surfaces are displayed in the **Supplementary Figure S1**. Smooth and even surface could be observed for the $Ca_2Nb_2O_7$ film, while bumps and hollows were present on the surface of nonstoichiometric films, with the highest degree of roughness obtained by the $Ca_2Nb_{1.9}O_{7-\delta}$ surface. The corresponding element mapping images show that the elements Ca and Nb from the $Ca_2Nb_2O_7$ films were uniformly distributed on the surface of STO substrate for all samples, while the element O exhibited higher degree of density due to the simultaneous contribution from the film and substrate.

Figure 2 shows the core level XPS for the $Ca_2Nb_2O_7$, $Ca_{1.9}Nb_2O_{7-\delta}$ and $Ca_2Nb_{1.9}O_{7-\delta}$ films. All spectra were charge

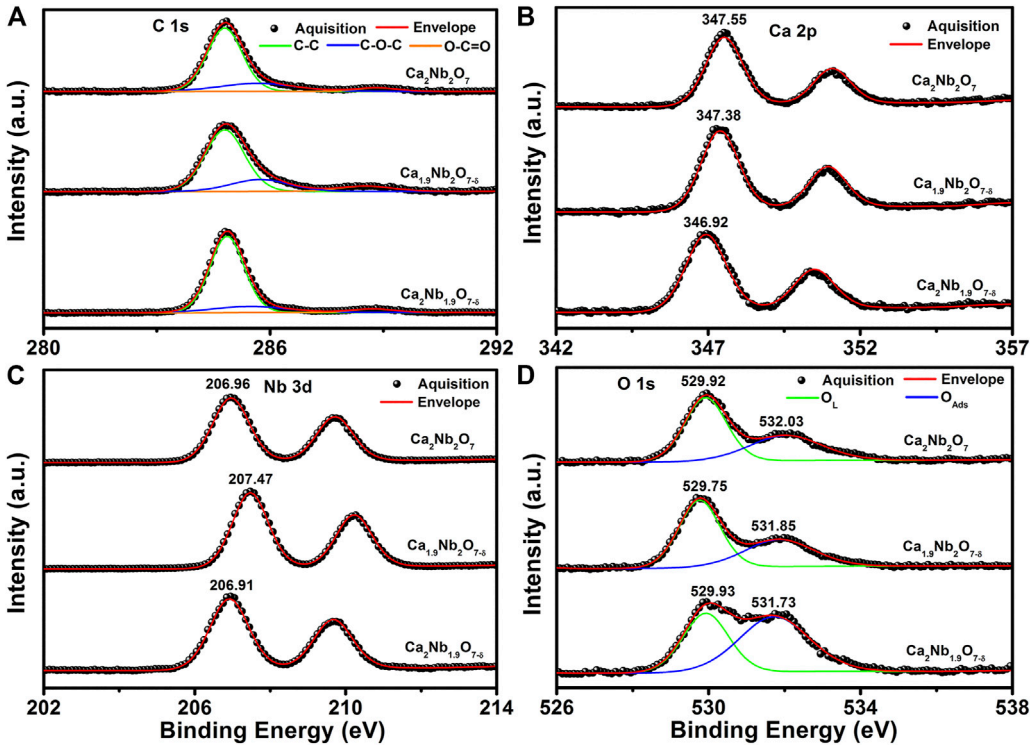

FIGURE 2 | C 1s **(A)**, Ca 2p **(B)**, Nb 3d **(C)** and O 1s **(D)** core level XPS for the $Ca_2Nb_2O_7$, $Ca_{1.9}Nb_2O_{7-\delta}$ and $Ca_2Nb_{1.9}O_{7-\delta}$ films.

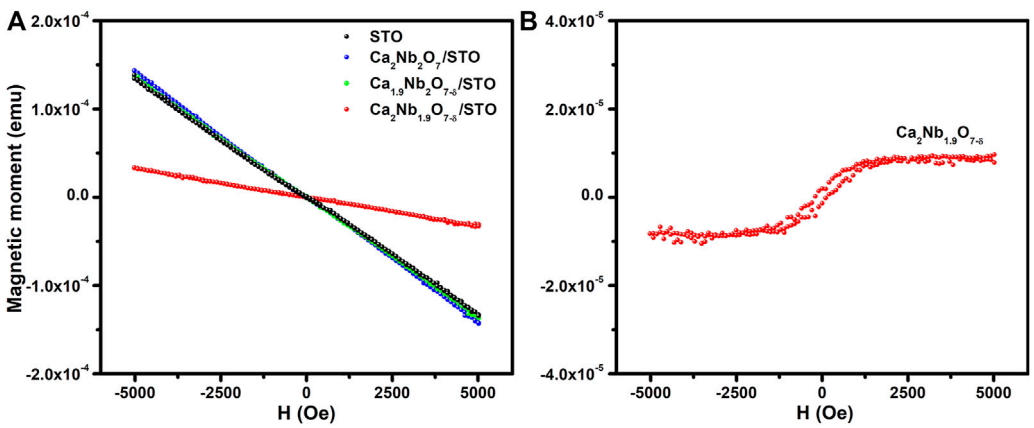

FIGURE 3 | Original MH curves for the STO substrate, $Ca_2Nb_2O_7$, $Ca_{1.9}Nb_2O_{7-\delta}$ and $Ca_2Nb_{1.9}O_{7-\delta}$ films on STO measured at room temperature **(A)**, and the MH curve for the $Ca_2Nb_{1.9}O_{7-\delta}$ film after subtraction of the diamagnetic signal from the substrate **(B)**.

corrected according to the C-C peak at the binding energy (BE) of 284.8 *e*V. In **Figure 2A**, the C-C and C-O-C peaks come from the adventitious carbon contamination, while the small amount of O-C=O peaks originate from the carbonate formed on the surface. From the Ca 2*p* and Nb 3*d* XPS in **Figures 2B,C**, Ca and Nb ions were in the valence states of +2 and +5 respectively. Since there is no other valence states present for Ca and Nb, the existence of Ca or Nb vacancy in the $Ca_2Nb_2O_7$ lattice can only induce oxygen vacancies to maintain the charge neutrality, hence the complex vacancy of V_{Ca+O} and V_{Nb+O} should be present in $Ca_{1.9}Nb_2O_{7-\delta}$ and $Ca_2Nb_{1.9}O_{7-\delta}$ films, respectively. With respect to the stoichiometric $Ca_2Nb_2O_7$ film, the $Ca_{1.9}Nb_2O_{7-\delta}$ film exhibited 0.17 *e*V lower BE for the Ca $2p_{3/2}$ peak but 0.51 *e*V higher BE for the Nb $3d_{5/2}$ peak, while the $Ca_2Nb_{1.9}O_{7-\delta}$ film exhibited 0.63 *e*V lower BE for the Ca $2p_{3/2}$ peak but 0.05 *e*V lower BE for the Nb $3d_{5/2}$ peaks. As for the O 1s XPS, lattice oxygen (O_L) and adsorbed oxygen (O_{ads}) were present in all samples, but the relative content of O_{ads} for the $Ca_2Nb_{1.9}O_{7-\delta}$ film

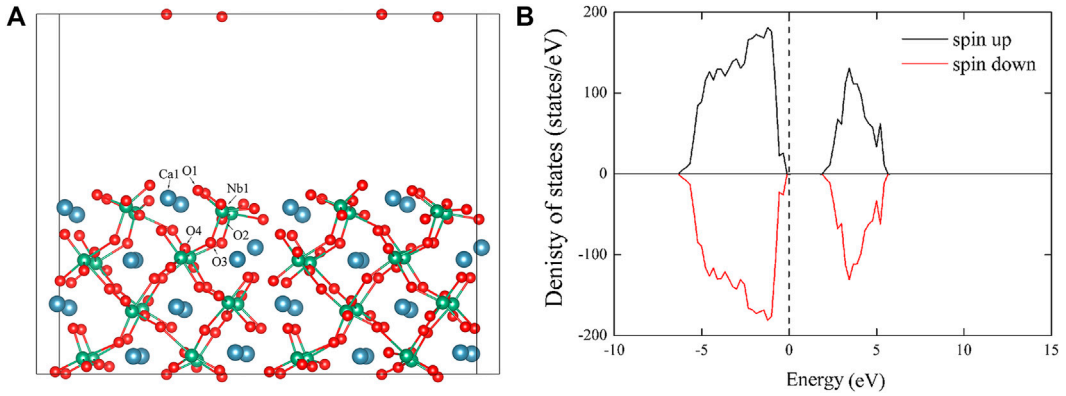

FIGURE 4 | Stable configuration of $Ca_2Nb_2O_7$ (010) surface with labeled Ca, Nb and O atoms to be removed for vacancy study **(A)**, and the total DOS of stoichiometric $Ca_2Nb_2O_7$ (010) surface **(B)**.

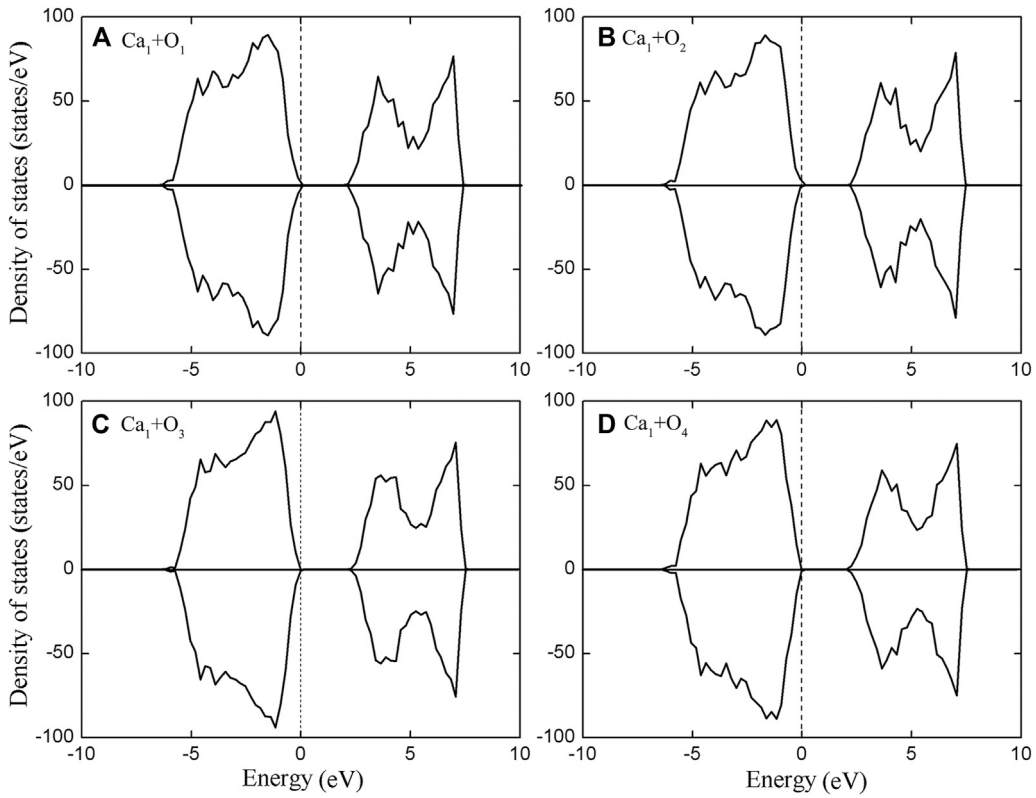

FIGURE 5 | DOSs of $Ca_2Nb_2O_7$ (010) surface with the complex vacancy of VCa+O in the distributions of Ca_1+O_1 **(A)**, Ca_1+O_2 **(B)**, Ca_1+O_3 **(C)**, and Ca_1+O_4 **(D)**.

was 58.8% which was much higher the 40.53 and 40.01% for the $Ca_2Nb_2O_7$ and $Ca_{1.9}Nb_2O_{7-\delta}$ films, respectively.

Magnetic Measurement

Figure 3 displays the MH curves for the STO substrate, $Ca_2Nb_2O_7$, $Ca_{1.9}Nb_2O_{7-\delta}$ and $Ca_2Nb_{1.9}O_{7-\delta}$ films on STO measured at room temperature. Compared with the diamagnetic behavior of the STO substrate, the stronger diamagnetic signals in the $Ca_2Nb_2O_7$ and $Ca_{1.9}Nb_2O_{7-\delta}$ films on STO suggest the presence of diamagnetism in the obtained films. However, the $Ca_2Nb_{1.9}O_{7-\delta}$ film on STO showed much weaker diamagnetic signal. As shown in **Figure 3B**, MH hysteresis loop was observed for the $Ca_2Nb_{1.9}O_{7-\delta}$ film after subtraction of the diamagnetic signal from the substrate, meaning that the $Ca_2Nb_{1.9}O_{7-\delta}$ film exhibited weak ferromagnetic behavior. Given the film thickness of 100 nm, the saturated magnetic moment of 9×10^{-6} emu corresponds to the magnetization of 3.6 emu/g for the $Ca_2Nb_{1.9}O_{7-\delta}$ film.

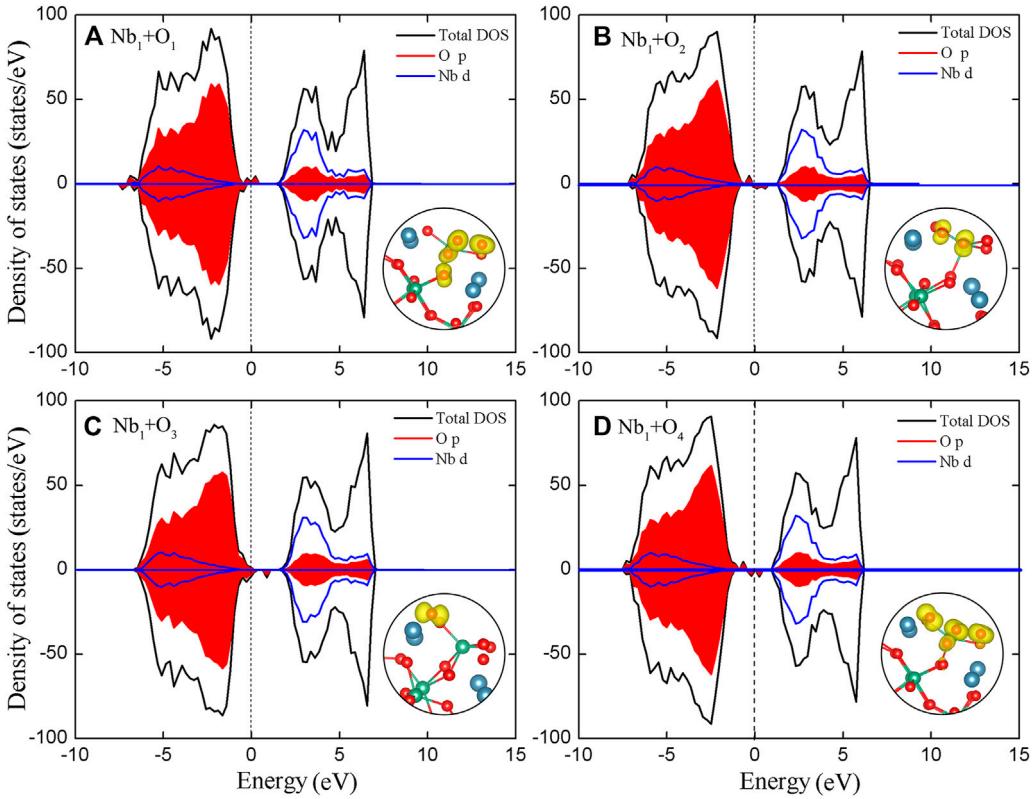

FIGURE 6 | Total and partial DOSs of $Ca_2Nb_2O_7$ (010) surface with the complex vacancy of VNb+O in the distributions of Nb_1+O_1 **(A)**, Nb_1+O_2 **(B)**, Nb_1+O_3 **(C)**, and Nb_1+O_4 **(D)**. The insets show the corresponding three-dimensional iso-surfaces of magnetization density.

Theoretical Calculation

In order to explore the origin of FM in the $Ca_2Nb_{1.9}O_{7-\delta}$ film, the density functional theory (DFT) calculations were performed using the plane-wave pseudopotential method in the Vienna Ab initio Simulation Package (VASP) (Kresse and Hafner, 1993a; Kresse and Joubert, 1999). The Projector Augmented Wave (PAW) (Kresse and Hafner, 1993b; Blöchl, 1994) potentials were employed, and General Gradient Approximate (GGA) was used to describe the exchange correlation energy. According to the XRD result, an orthorhombic $Ca_2Nb_2O_7$ $1 \times 2 \times 1$ supercell containing 176 atoms was first relaxed to get the most stable structure (see **Supplementary Figure S2A**) until the total energy in the optimized structure was converged to 1.0×10^{-4} *e*V/atom and the Hellman-Feynman force was smaller than 0.01 *e*V/Å. Then four different (010) planes were cleaved along the *b* axis, and a 10Å vacuum layer which was thick enough to isolate the atom layers was added above the supercell for further optimization. Among the four (010) surfaces, the configuration in the **Supplementary Figure S2B** showed the lowest energy, on which further calculations were performed.

The stable configuration of $Ca_2Nb_2O_7$ (010) surface with labeled Ca, Nb, and O atoms to be removed for vacancy study is displayed in **Figure 4A**, among which O1 is connected only to one Nb atom, O2 is coordinated between two neighbored Nb atoms, O3 connects one Nb atom in the outermost layer with another Nb atom in the second layer, while O4 denote the one between two Nb atoms in the second layer. Stoichiometric $Ca_2Nb_2O_7$ (010) surface was firstly studied and the total DOS was showed in **Figure 4B**. No spin polarization could be observed around the Fermi level, meaning that the stoichiometric $Ca_2Nb_2O_7$ (010) surface is nonmagnetic.

The complex vacancy of V_{Ca+O} in four different distributions, i.e., Ca1+O1, Ca1+O2, Ca1+O3, and Ca1+O4, was then studied. The relative stability (ΔE) of the $Ca_2Nb_2O_7$ (010) surface with these four types of complex vacancy was 3.51, 4.18, 0, and 2.21 *e*V respectively, meaning that the system with V_{Ca1+O3} was most stable. However, no spin polarization could be observed in the DOSs around the Fermi level in **Figure 5**, indicating that the complex vacancy of V_{Ca+O} cannot induce magnetism in the $Ca_2Nb_2O_7$ (010) surface. On the other side, the complex vacancy of V_{Nb+O} in four different distributions all induced spin polarization around the Fermi level and impurity bands in the forbidden gap (see **Figure 6**), which were contributed mainly by the O 2*p* electrons. The three-dimensional iso-surfaces of magnetization density in the inset of **Figure 6** show that the complex vacancies of V_{Nb+O} mainly induced spin polarization on the residual O atoms around the Nb vacancies. The total net magnetic moment (M_{tot}) of the system with V_{Nb1+O1}, V_{Nb1+O2}, V_{Nb1+O3}, and V_{Nb1+O4} was 1.0, 0.99, 0.96, and 1.0 μ_B, respectively. Among which, the system with V_{Nb1+O4} was the most stable one with the lowest energy, and the ΔE of the system with V_{Nb1+O1}, V_{Nb1+O2} and V_{Nb1+O3} was 1.04, 27.46, and 27.90 *e*V,

respectively. More importantly, FM coupling was energetically more favorable than AFM coupling in the cases of V_{Nb1+O1} and V_{Nb1+O4}, with the relative energy between FM and AFM as 7 and 45 m*e*V, respectively.

CONCLUSION

Nonstoichiometric $Ca_2Nb_2O_7$ single phase films with the complex vacancy of V_{Ca+O} or V_{Nb+O} were deposited on STO (110) substrate under appropriate deposition conditions using nonstoichiometric ceramic targets. The V_{Ca+O} cannot induce magnetism in the diamagnetic stoichiometric $Ca_2Nb_2O_7$ (020) single phase film, while V_{Nb+O} can induce spin polarization on the residual O atoms around the Nb vacancies, and make the $Ca_2Nb_2O_7$ film exhibit FM behavior at RT. Our work demonstrated experimentally and theoretically that the introduction of intrinsic complex vacancy during deposition should be a feasible way to induce ferromagnetism in the ferroelectric $Ca_2Nb_2O_7$ film, and this method might be applicable to other $A_2Nb_2O_7$-type niobate ferroelectric films as well.

DATA AVAILABILITY STATEMENT

The original contributions presented in the study are included in the article/**Supplementary Material**, further inquiries can be directed to the corresponding author.

AUTHOR CONTRIBUTIONS

EC contributed to conception and design of the study. LW, YZ and ZN contributed to the acquisition, analysis and interpretation of data. All authors contributed to manuscript revision, read, and approved the submitted version.

FUNDING

This work was supported by National Natural Science Foundation of China (11404236, 11604236, and 11974258), Natural Science Foundation of Shanxi Province (201901D111117 and 201901D111126).

ACKNOWLEDGMENTS

Part of this study has been performed using facilities at IBS Center for Correlated Electron Systems, Seoul National University.

SUPPLEMENTARY MATERIAL

The Supplementary Material for this article can be found online at: https://www.frontiersin.org/articles/10.3389/fmats.2021.736011/full#supplementary-material

REFERENCES

Blöchl, P. E. (1994). Projector Augmented-Wave Method. *Phys. Rev. B* 50, 17953–17979. doi:10.1103/physrevb.50.17953

Cao, D., Cai, M.-Q., Hu, W.-Y., Yu, P., and Huang, H.-T. (2011). Vacancy-induced Magnetism in BaTiO3(001) Thin Films Based on Density Functional Theory. *Phys. Chem. Chem. Phys.* 13, 4738–4745. doi:10.1039/c0cp02424d

Cao, D., Cai, M. Q., Zheng, Y., and Hu, W. Y. (2009). First-principles Study for Vacancy-Induced Magnetism in Nonmagnetic Ferroelectric BaTiO3. *Phys. Chem. Chem. Phys.* 11, 10934–10938. doi:10.1039/b908058a

Cao, E., Hu, J., Qin, H., Ji, F., Zhao, M., and Jiang, M. (2011). Room Temperature Ferromagnetism and Magnetoelectric Coupling in (K0.5Na0.5)NbO3 PLD Nanocrystalline Films. *J. Alloys Comp.* 509, 2914–2918. doi:10.1016/j.jallcom.2010.11.155

Cao, E., Zhang, Y., Ju, L., Sun, L., Qin, H., and Hu, J. (2012). The Investigation of Room Temperature Ferromagnetism in (100) Oriented BaNb2O6 PLD Films on LaAlO3 (100) Substrate. *Appl. Surf. Sci.* 258, 3795–3799. doi:10.1016/j.apsusc.2011.12.031

Cao, E., Zhang, Y., Qin, H., Zhang, L., and Hu, J. (2013). Vacancy-induced Magnetism in Ferroelectric LiNbO3 and LiTaO3. *Physica. B. Condens. Matter* 410, 68–73. doi:10.1016/j.physb.2012.10.030

Chand Verma, K., Kaur, J., Negi, N. S., and Kotnala, R. K. (2014). Multiferroic and Magnetoelectric Properties of Nanostructured BaFe0.01Ti0.99O3 Thin Films Obtained under Polyethylene Glycol Conditions. *Solid State. Commun.* 178, 11–15. doi:10.1016/j.ssc.2013.10.020

Chun, S. H., Chai, Y. S., Jeon, B. G., Kim, H. J., Oh, Y. S., Kim, I., et al. (2012). Electric Field Control of Nonvolatile Four-State Magnetization at Room Temperature. *Phys. Rev. Lett.* 108, 177201. doi:10.1103/physrevlett.108.177201

Díaz-Moreno, C. A., Farías-Mancilla, R., Matutes-Aquino, J. A., Elizalde-Galindo, J., Espinosa-Magaña, F., González-Hernández, J., et al. (2014). Magnetic Behavior in LiNbO3 Nanocrystallites Caused by Oxygen Vacancies. *J. Magnetism Magn. Mater.* 356, 82–86. doi:10.1016/j.jmmm.2013.12.029

Fiebig, M. (2005). Revival of the Magnetoelectric Effect. *J. Phys. D. Appl. Phys.* 38, R123–R152. doi:10.1088/0022-3727/38/8/r01

Hill, N. A. (2000). Why Are There So Few Magnetic Ferroelectrics? *J. Phys. Chem. B* 104, 6694–6709. doi:10.1021/jp000114x

Kresse, G., and Hafner, J. (1993). Ab Initiomolecular Dynamics for Liquid Metals. *Phys. Rev. B* 47, 558–561. doi:10.1103/physrevb.47.558

Kresse, G., and Hafner, J. (1993). Ab Initiomolecular Dynamics for Open-Shell Transition Metals. *Phys. Rev. B* 48, 13115–13118. doi:10.1103/physrevb.48.13115

Kresse, G., and Joubert, D. (1999). From Ultrasoft Pseudopotentials to the Projector Augmented-Wave Method. *Phys. Rev. B* 59, 1758–1775. doi:10.1103/physrevb.59.1758

Li, Y. D., Wang, C. C., Cheng, R. L., Lu, Q. L., Huang, S. G., and Liu, C. S. (2014). Vacancy-driven Magnetism in Nonmagnetic Double Perovskite Sr2AlNbO6: A First-Principles Study. *J. Alloys Comp.* 598, 1–5. doi:10.1016/j.jallcom.2014.01.176

Lichtenberg, F., Herrnberger, A., Wiedenmann, K., and Mannhart, J. (2001). Synthesis of Perovskite-Related Layered AnBnO3n+2 = ABOX Type Niobates and Titanates and Study of Their Structural, Electric and Magnetic Properties. *Prog. Solid State. Chem.* 29, 1–70. doi:10.1016/s0079-6786(01)00002-4

Liu, L., Shi, D., Fan, L., Chen, J., Li, G., Fang, L., et al. (2015). Ferroic Properties of Fe-Doped and Cu-Doped K0.45Na0.49Li0.06NbO3 Ceramics. *J. Mater. Sci. Mater. Electron.* 26, 6592–6598. doi:10.1007/s10854-015-3257-z

Mangalam, R. V. K., Ray, N., Waghmare, U. V., Sundaresan, A., and Rao, C. N. R. (2009). Multiferroic Properties of Nanocrystalline BaTiO3. *Solid State. Commun.* 149, 1–5. doi:10.1016/j.ssc.2008.10.023

Ramana, E. V., Yang, S. M., Jung, R., Jung, M. H., Lee, B. W., and Jung, C. U. (2013). Ferroelectric and Magnetic Properties of Fe-Doped $BaTiO_3$ Thin Films Grown by the Pulsed Laser Deposition. *J. Appl. Phys.* 113, 187219. doi:10.1063/1.4801965

Shimada, T., Uratani, Y., and Kitamura, T. (2012). Vacancy-driven Ferromagnetism in Ferroelectric PbTiO3. *Appl. Phys. Lett.* 100, 162901. doi:10.1063/1.4704362

Song, Y.-J., Zhang, Q.-H., Shen, X., Ni, X.-D., Yao, Y., and Yu, R.-C. (2014). Room-Temperature Magnetism Realized by Doping Fe into Ferroelectric $LiTaO_3$. *Chin. Phys. Lett.* 31, 017501. doi:10.1088/0256-307x/31/1/017501

Topkaya, R., Boyraz, C., and Ekmekçi, M. K. (2017). Structural and Magnetic Properties of Eu^{3+}-Doped $CdNb_2O_6$ Powders. *J. Low Temp. Phys.* 190, 244–255. doi:10.1007/s10909-017-1835-6

Yang, F., Jin, K., Lu, H., He, M., Wang, C., Wen, J., et al. (2010). Oxygen Vacancy Induced Magnetism in BaTiO3−δ and Nb:BaTiO3−δ Thin Films. *Sci. China Phys. Mech. Astron.* 53, 852–855. doi:10.1007/s11433-010-0187-x

Conflict of Interest: The authors declare that the research was conducted in the absence of any commercial or financial relationships that could be construed as a potential conflict of interest.

The handling Editor declared a past co-authorship with one of the authors NZ.

Publisher's Note: All claims expressed in this article are solely those of the authors and do not necessarily represent those of their affiliated organizations, or those of the publisher, the editors and the reviewers. Any product that may be evaluated in this article, or claim that may be made by its manufacturer, is not guaranteed or endorsed by the publisher.